The Nature of Aqueous Tunneling Pathways Between Electron-Transfer Proteins

Jianping Lin, Ilya A. Balabin, and David N. Beratan[*]

Departments of Chemistry and Biochemistry

Duke University

Durham, NC 27708

SUPPORTING MATERIAL

1. System setup and MD Simulations. The structure of cytochrome b_5 was taken from the PDB entry 1CYO *(1)*. One non-crystallographic water molecule was added using the DOWSER program *(2)*. For each simulated system geometry (i.e., for each combination of a porphyrin angle and a distance between rings), the cytochrome b_5 molecules were solvated in a TIP3 water box with a 7 Å distance between the molecule and the box surface using the Solvate plugin *(3)* for the program VMD *(4)*. Sodium and chlorine counter-ions were added to an ionic strength of 0.2*M* using the Meadionize plugin *(5, 6)*, a modified

version of the Autoionize plugin *(7)* for VMD. The ions were placed at the minima of the electrostatic potential map, maintaining a minimum distance of 5 Å between any ion and protein as well as between any two ions *(5)*. Each system was minimized for 1,000 steps and equilibrated for 200ps using the Charmm27 forcefield *(8)*, NpT ensemble, periodic boundary conditions, and particle-mesh Ewald full electrostatics calculations *(9)*. Atomic partial charges on the heme group in the oxidized state were modeled assuming that the additional positive charge is uniformly distributed over the heme iron ion and six nitrogen atoms in contact with it *(10)*. In order to maintain the orientation and distance between the porphyring rings, the MD simulations were performed using harmonic restraints imposed on the heavy atoms of the porphyrin rings and on the protein backbone. The NAMD2 molecular dynamics program *(11)* was used.

Water density in the inter-protein space was monitored during the MD simulations. For each system conformation in each simulation, the density was estimated by counting the number of water molecule oxygen atoms located in a cylinder with the axis on the line connecting the two iron ions in the hemes, length from one heme group to the other, and radius of 4, 7, or 10 Å (to eliminate possible dependence of the estimated density on the cylinder radius used). The results are shown in Fig. S6, where the data points represent the average densities over the MD trajectories, and the error bars represent the sampling error estimated using the renormalization group-based approach *(17)*. To estimate whether the water distribution during the simulations was equilibrium, regression analysis was used to compute the overall change in the water density

over entire length of the MD simulations. This change turned out to be random in sign and small in magnitude: average over all donor-to-acceptor distances change was only about 3, 7, and 19% of the RMS fluctuations of the density for porphyrin angles of 0^o, 45^o, and 90^o, respectively. The overall change in T_{DA}^2 was estimated in the same way and turned out to be 8, 19, and 10% of the RMS fluctuations of T_{DA}^2 for porphyrin angles of 0^o, 45^o, and 90^o, respectively. The fact that the overall changes in water density and T_{DA}^2 over the entire length of the simulations are much smaller than the RMS fluctuations of these quantities indicates that the simulations were done in the equilibrium regime.

2. Electronic coupling calculations. The donor-acceptor electronic coupling T_{DA} was computed in the superexchange ET regime *(12)* using an extended Hückel-level Hamiltonian parameterized from density functional calculations *(13)*:

$$T_{DA} = \sum_{\mu,\nu} (E_{tun} S_{D\mu} - H_{D\mu})(E_{tun} S_{\mu\nu} - H_{\mu\nu})^{-1} (E_{tun} S_{\nu A} - H_{\nu A}) . \qquad (1)$$

E_{tun} is the electron tunneling energy, **S** and **H** are the overlap and Hamiltonian matrices, respectively, the index D (A) refers to the donor (acceptor) orbitals, and Greek indices refer to bridge orbitals. Following *(14)*, the To incorporate effects of the protein thermal motion on the donor (acceptor) orbitals, the latter were defined for each snapshot of the MD trajectory as the HOMO's computed for truncated heme groups (not including the histidine ligands, propionates, methyl groups, and hydrogen atoms) and were dominantly localized on the Fe ions. tunneling energy was set to –9.9*eV*. To account for mixing of the initial and final

states with the bridge, the coupling was scaled using the method described in refs. *(15, 16)*. The sampling error in the T_{DA} calculations was estimated using a renormalization group-based method described in ref. *(18)*.

Since the autocorrelation time of T_{DA} has recently been found to lie in the tens of femtoseconds range (ref. 18 in the report), the T_{DA} values computed with the 1ps interval were assumed independent.

The short distance coupling decays (Figs. S1-S3) are smaller than one would expect for pure vacuum tunneling. This likely arises because the dominant protein-mediated portions of the tunneling pathways change as the proteins separate. As such, increasing the distance between proteins does not lead to a simple linear increase in the vacuum tunneling distance and, therefore, produces a tunneling distance decay intermediate between pure through-bond and pure values.

3. Cytochrome b_5 self-exchange rate calculation. The bimolecular rates were computed using the Brownian dynamics approach of Northrup and co-workers *(18)*. The single-exponential decay model used in *(18)* was replaced with a three-exponent model (Fig. S4, eq. 3):

$$k_{et}(d) = \begin{cases} k_{et}^{0} \exp(-\beta_1 (d - d_0)) & 5.17\text{Å} \le d < 9.0\text{Å} \\ k_{et}^{0} \exp(-\beta_1 (9.0 - d_0)) & 9.0\text{Å} \le d < 12.0\text{Å} \\ k_{et}^{0} \exp(-\beta_1 (9.0 - d_0)) \exp(-\beta_2 (d - 12.0)) & 12.0\text{Å} \le d \end{cases}, \quad (2)$$

where $k_{et}(d)$ is the intrinsic ET rate constant for a distance d between the porphyrin ring edges, and d_0 = 5.17 Å is the distance between the two porphyrin

rings when the proteins are in the contact. The three decay exponents were estimated by averaging the XH coupling data over the corresponding distance ranges, leading to β_1~1.5 Å^{-1} for the direct contact regime (for co-planar porphyrin rings). The ET rates in the structured water mediated regime were assumed distance-independent. In the bulk water regime, β_2 was dependent on the protein orientation, varying from 2.5 to 3.6 Å^{-1}. However, these variations only cause a 20% change in the computed bimolecular rate, indicating that the latter is predominantly controlled by the structured water ET regime. We used β_2 = 2.5 Å^{-1} in the bimolecular ET rate calculations.

Following *(19)*, k_{et}^0 is defined as

$$k_{et}^0 = \frac{4\pi^2}{h} \left|T_{DA}(d_0)\right|^2 \frac{\exp[-(\Delta G^0 + \lambda)^2 / 4\lambda k_B T]}{\sqrt{4\pi\lambda k_B T}} \quad , \qquad (3)$$

where the reorganization energy λ is set to 1.2eV *(20)*, and the temperature T is 300K. For self-exchange, the driving force ΔG^0 is zero. The squared electronic coupling T_{DA}^2 at contact is estimated to be about 1.69×10^{-3} eV^2 (s-Fig. 1, curve A), and the corresponding ET rate k_{et}^0 is 2.4×10^8 s^{-1}. All bimolecular rate constants were calculated using the modified Brownian dynamics program SDA *(21)* as described in ref. *(22)*.

References

1. R. C. E. Durley, F. S. Mathews, *Acta Cryst.* **D52**, 65 (1996).

2. http://hekto.med.unc.edu:8080/HERMANS/software/DOWSER/Dowser.htm

3. http://www.ks.uiuc.edu/Research/vmd/plugins/solvate/

4. http://www.ks.uiuc.edu/Research/vmd

5. http://www.chem.duke.edu/~ilya/software/meadionize.html

6. http://www.scripps.edu/mb/bashford/

7. http://www.ks.uiuc.edu/Research/vmd/plugins/autoionize/

8. A. D. Mackerell *et al*, *J. Phys. Chem.* **B102**, 3586 (1998).

9. T. Darden, D. York, L. Pedersen, *J. Chem. Phys.* **98**, 10089 (1993).

10. Q. Wang, C. F. Wong, H. Rabitz, *Biophys. J.* **75**, 60 (1998).

11. http://www.ks.uiuc.edu/Research/namd

12. S. Priyadarshy, S. S. Skourtis, S. M. Risser, D. N. Beratan, *J. Chem. Phys.* **104**, 9473 (1996).

13. A. Vela, J. L. Gazquez, *J. Phys. Chem.* **92**, 5688 (1988).

14. I. A. Balabin, J. N. Onuchic, *Science* **290**, 114 (2000).

15. W. T. Yip, D. H. Levy, R. Kobetic, P. Piotrowiak, *J. Phys. Chem.* **A103**, 10 (1999).

16. T. Kawatsu, T. Kakitani, T. Yamato, *J. Phys. Chem. B* **106**, 5068 (2002).

17. H. Flyvbjerg, H. G. Petersen, *J. Chem. Phys.* **91**, 461 (1989).

18. S. M. Andrew, K. A. Thomasson, S. H. Northrup, *J. Am. Chem. Soc.* **115**, 5516 (1993).

19. R. A. Marcus, N. Sutin, *Biochim. Biophys. Acta* **811**, 265 (1985).

20. D. W. Dixon, X. Hong, S. E. Woehler, A. G. Mauk, B. P. Sishta, *J. Am. Chem. Soc.* **112**, 1082 (1990).

21. R. R. Gabdoulline, R. C. Wade, *Methods* **14**, 329 (1998).

22. J. Lin, D. N. Beratan, *J. Phys. Chem. B* **109**, 7529 (2005).

Figure Captions:

Figure S1. The mean square electronic coupling dependence on the distance between the two porphyrin rings (90º angle between porphyrin rings): XH(P,W) - proteins and water, extended-Hückel (XH) calculations; XH(P) - proteins only, XH calculations; PW(P,W) - proteins and water, *Pathways* model analysis; PW(P) - proteins only, *Pathways* model analysis; PD(P,W) - proteins and water, packing density estimates; PD(P) - proteins only, packing density estimates. The three distance ranges correspond to the direct contact regime, structured water mediated regime, and bulk water mediated regime, respectively. The error bars show the sampling error estimated using a renormalization group based method (17).

Figure S2. The mean square electronic coupling dependence on the distance between the two porphyrin rings (0º angle between porphyrin rings): XH(P,W) - proteins and water, extended-Hückel (XH) calculations; XH(P) - proteins only, XH calculations; PW(P,W) - proteins and water, *Pathways* model analysis; PW(P) - proteins only, *Pathways* model analysis; PD(P,W) - proteins and water, packing density estimates; PD(P) - proteins only, packing density estimates. The three distance ranges correspond to the direct contact regime, structured water mediated regime, and bulk water mediated regime, respectively. The error bars show the sampling error estimated using a renormalization group based method (17).

Figure S3. The mean square electronic coupling dependence on the distance between the two porphyrin rings (45º angle between porphyrin rings): XH(P,W) - proteins and water, extended-Hückel (XH) calculations; XH(P) - proteins only, XH calculations; PW(P,W) - proteins and water, *Pathways* model analysis; PW(P) - proteins only, *Pathways* model analysis; PD(P,W) - proteins and water, packing density estimates; PD(P) - proteins only, packing density estimates. The three distance ranges correspond to the direct contact regime, structured water mediated regime, and bulk water mediated regime, respectively. The error bars show the sampling error estimated using a renormalization group based method (17).

Figure S4. A schematic view of the three-exponential model derived from the extended- Hückel analysis of the solvated proteins.

Figure S5. The mean square electronic coupling dependence on the distance between the two porphyrin rings (90º angle between porphyrin rings) for different donor and acceptor orbitals, extended-Hückel calculations. XH(P,W,H) - proteins and water, extended-Hückel (XH) calculations, donor and acceptor orbitals on the heme porphyrin ring; XH(P,H) - proteins only, XH calculations donor and acceptor orbitals on the heme porphyrin ring; XH(P,W,I) - proteins and water, extended-Hückel (XH) calculations, donor and acceptor orbitals on the iron ion; XH(P,I) - proteins only, XH calculations donor and acceptor orbitals on the iron ion. The three distance ranges correspond to the direct contact regime,

structured water mediated regime, and bulk water mediated regime, respectively. The error bars show the sampling error estimated using a renormalization group-based method (17).

Figure S6. Interprotein water density *vs.* interprotein distance for porphyrin angles of 0^o (top panel), 45^o (middle panel), and 90^o (bottom panel), respectively.

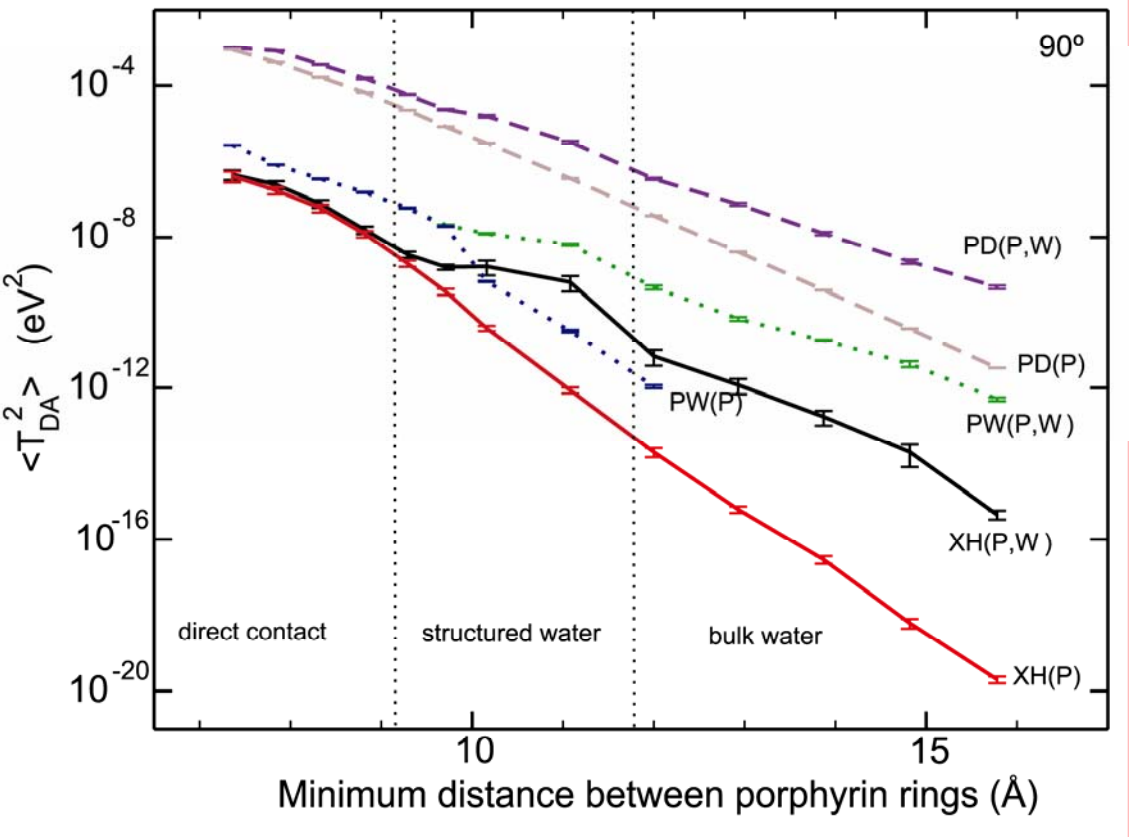
90º
PD(P,W)
PD(P)
PW(P)
PW(P,W)
XH(P,W)
XH(P)
direct contact
structured water
bulk water
10^{-4}
10^{-8}
10^{-12}
10^{-16}
10^{-20}
$<T^2_{DA}>$ (eV^2)
10
15
Minimum distance between porphyrin rings (Å)

Figure S1.

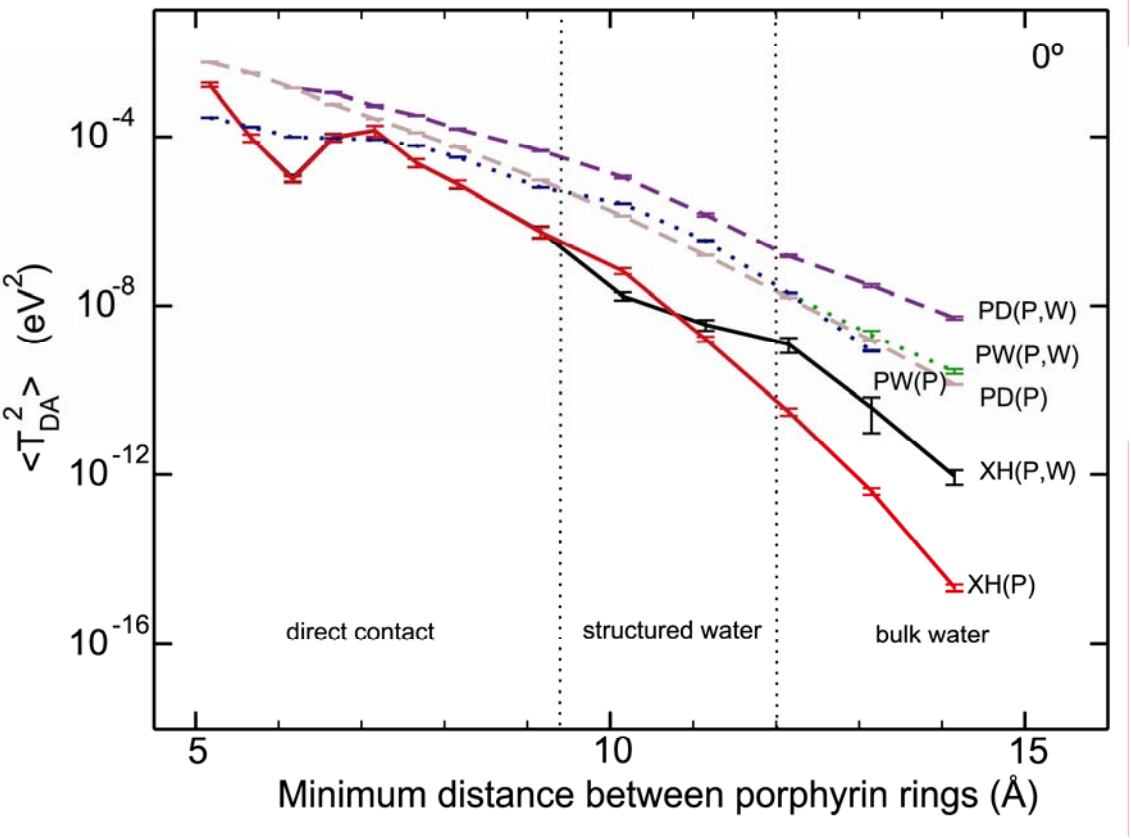
0°
10^{-4}
10^{-8}
10^{-12}
10^{-16}
$<T^2_{DA}>$ (eV^2)
PD(P,W)
PW(P,W)
PW(P)
PD(P)
XH(P,W)
XH(P)
direct contact
structured water
bulk water
5
10
15
Minimum distance between porphyrin rings (Å)

Figure S2.

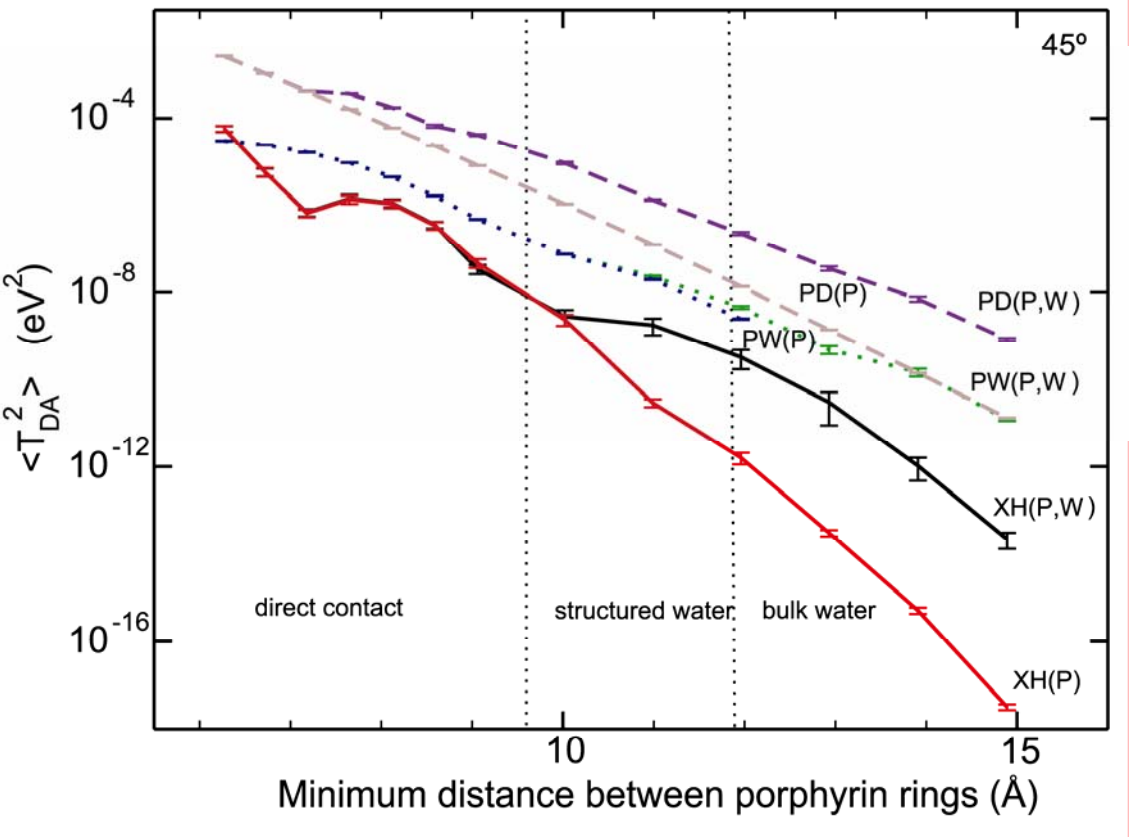
45º
10^{-4}
10^{-8}
10^{-12}
10^{-16}
$<T^2_{DA}>$ (eV^2)
PD(P)
PD(P,W)
PW(P)
PW(P,W)
XH(P,W)
XH(P)
direct contact
structured water
bulk water
10
15
Minimum distance between porphyrin rings (Å)

Figure S3.

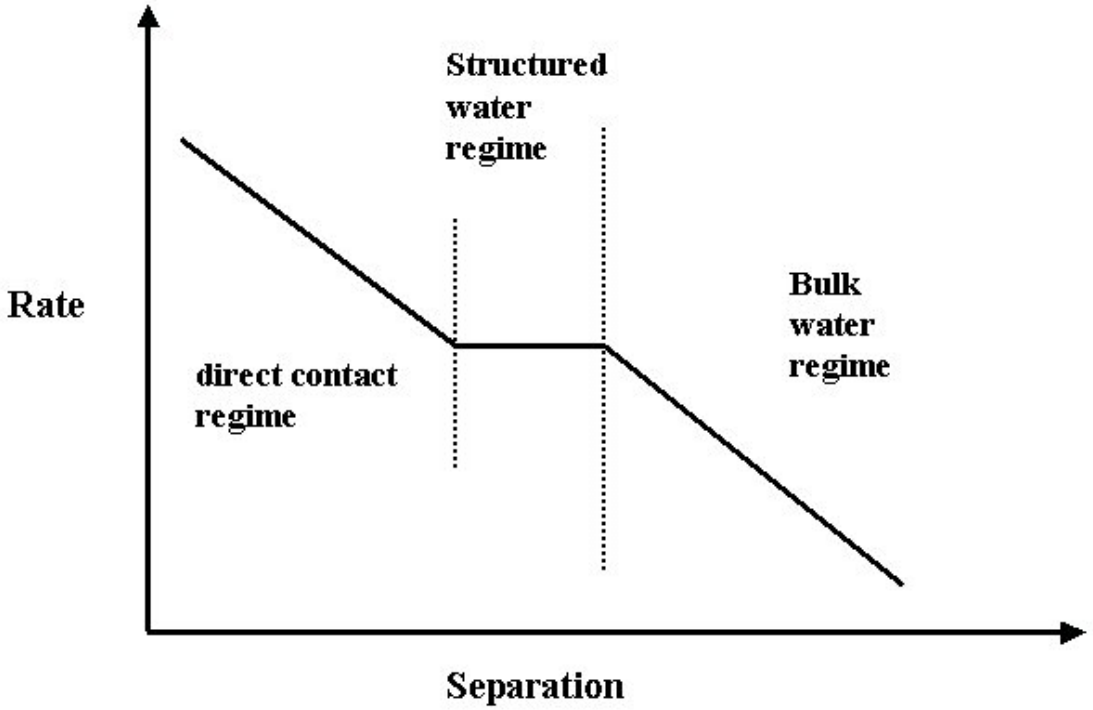
Structured
water
regime
Rate
Bulk
water
regime
direct contact
regime
Separation

Figure S4.

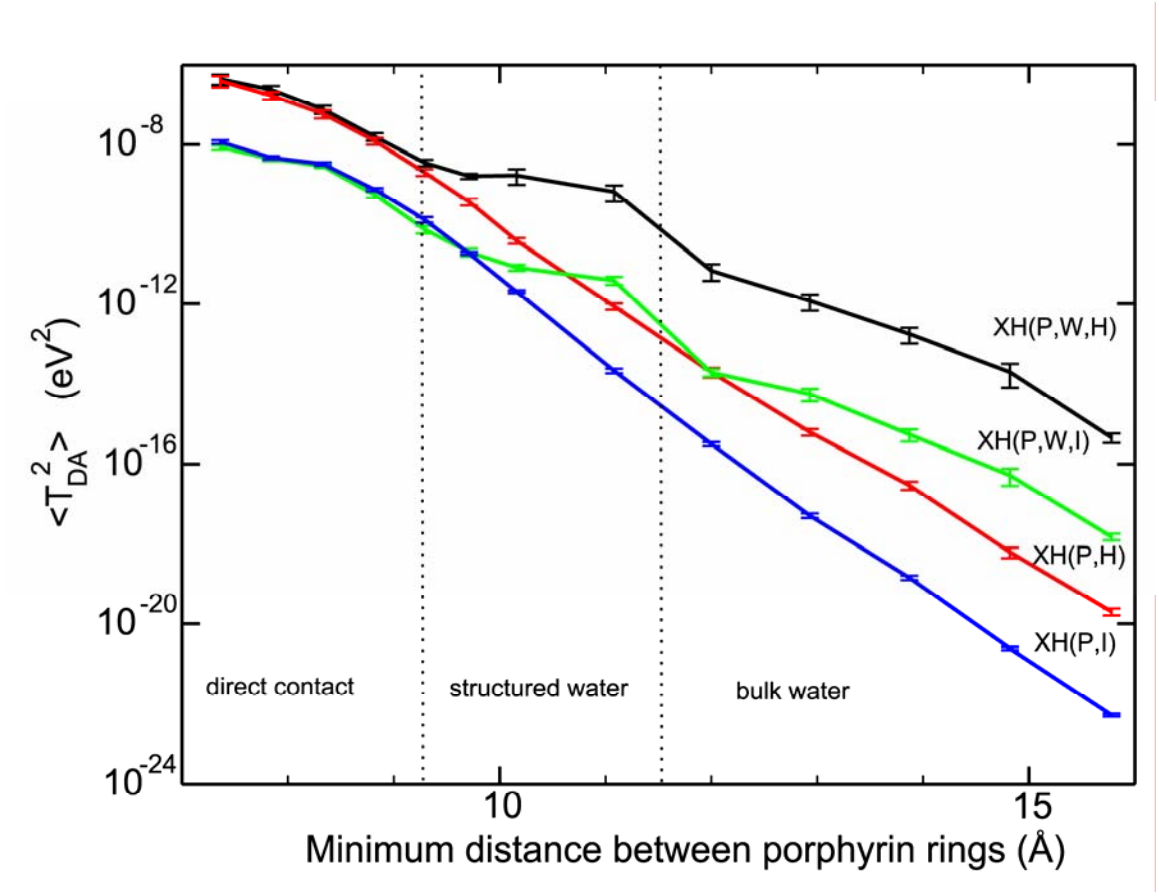
10^{-8}
10^{-12}
10^{-16}
10^{-20}
10^{-24}
$<T_{DA}^2>$ (eV^2)
XH(P,W,H)
XH(P,W,I)
XH(P,H)
XH(P,I)
direct contact
structured water
bulk water
10
15
Minimum distance between porphyrin rings (Å)

Figure S5.

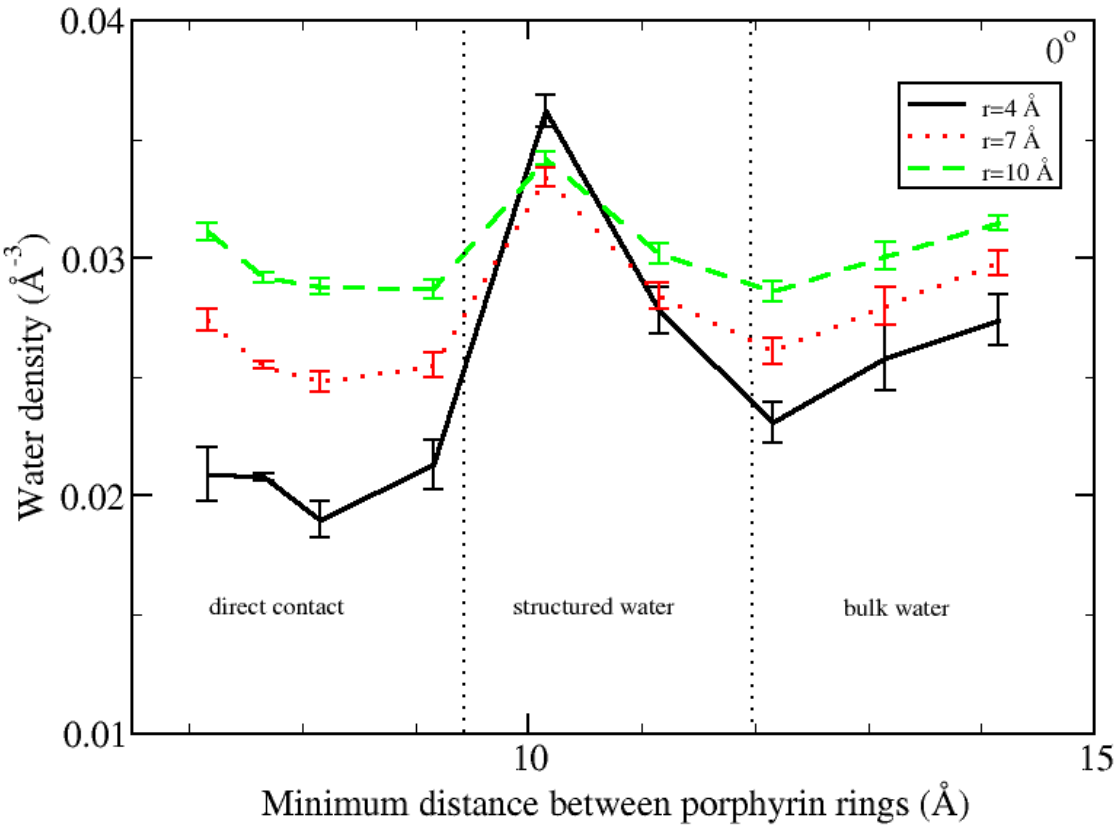
0.04
0.03
0.02
0.01
Water density (Å^{-3})
10
15
Minimum distance between porphyrin rings (Å)
0°
r=4 Å
r=7 Å
r=10 Å
direct contact
structured water
bulk water

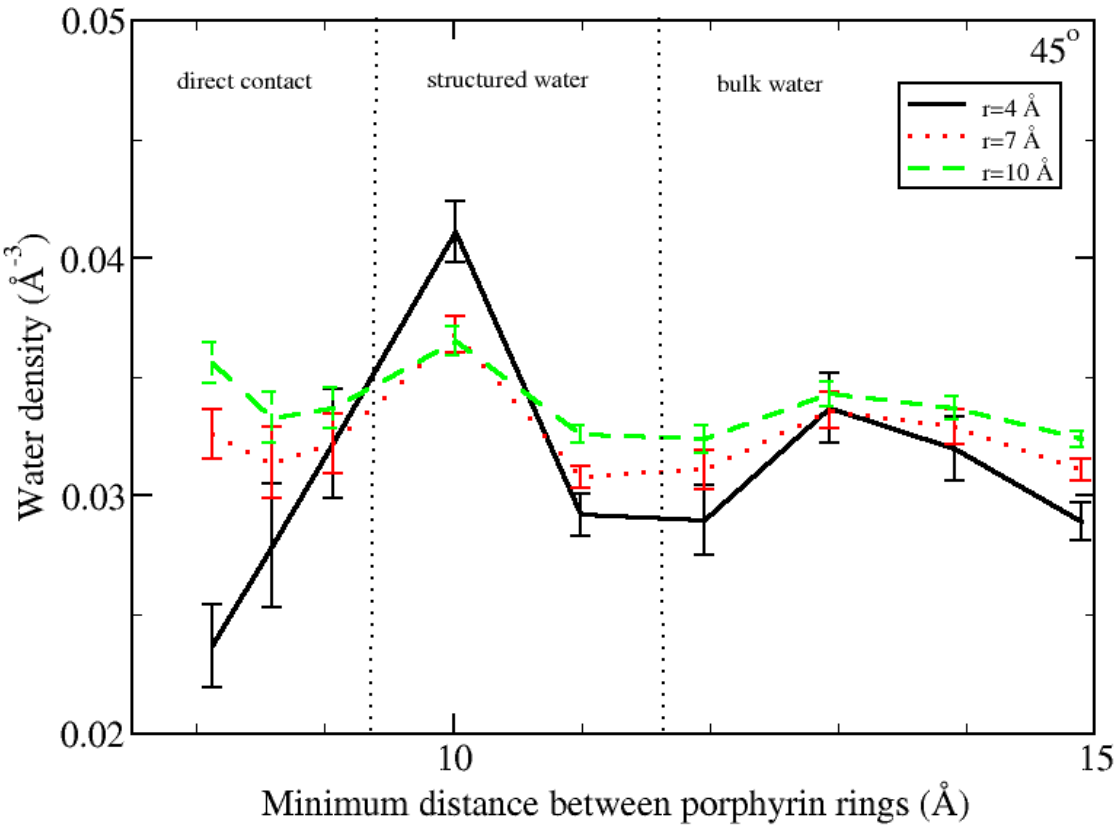
0.05
0.04
0.03
0.02
Water density (Å^{-3})
direct contact
structured water
bulk water
45°
r=4 Å
r=7 Å
r=10 Å
10
15
Minimum distance between porphyrin rings (Å)

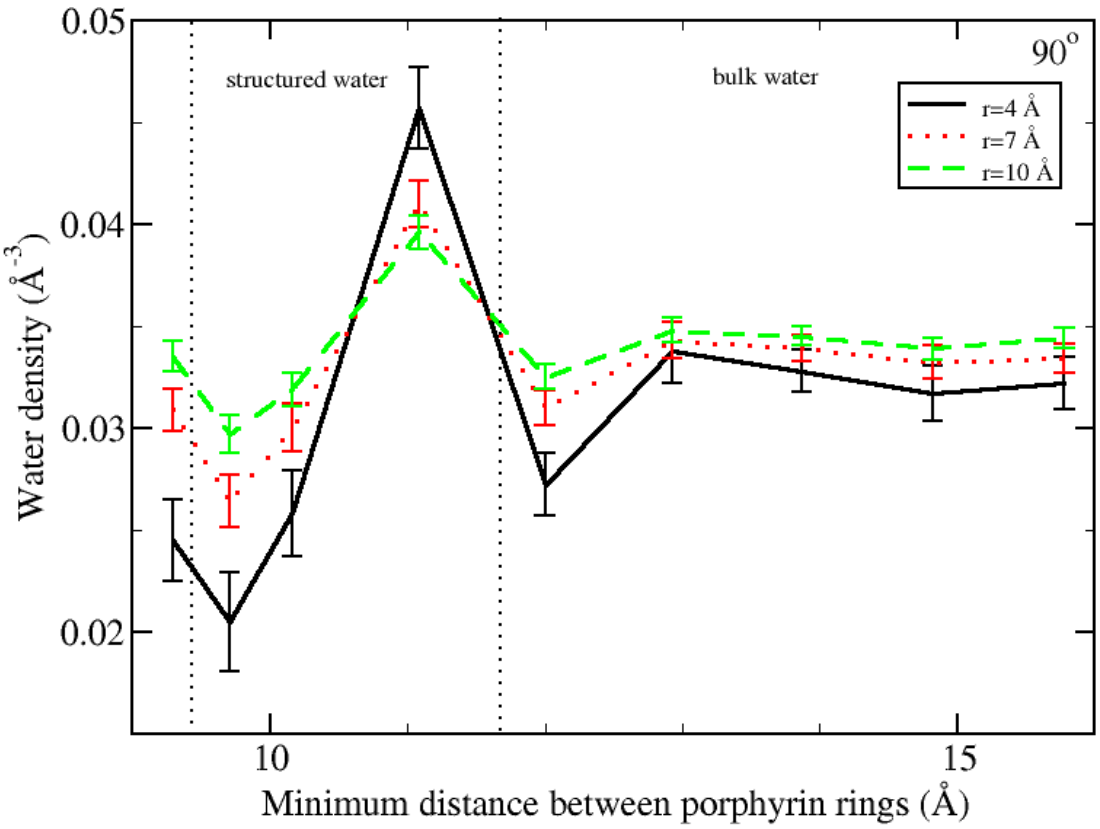
0.05
0.04
0.03
0.02
Water density (Å^{-3})
structured water
bulk water
90°
r=4 Å
r=7 Å
r=10 Å
10
15
Minimum distance between porphyrin rings (Å)

Figure S6.